Japanese Journal of Applied Physics

BRIEF NOTE

Evaluation of error factors depending on ultrasonic transmitted beamwidth in measurement of myocardial minute velocity

Japanese Journal of Applied Physics **60**, SDDE05 (2021) **BRIEF NOTE**
https://doi.org/10.35848/1347-4065/abef0e

Evaluation of error factors depending on ultrasonic transmitted beamwidth in measurement of myocardial minute velocity

Kana Sugahara[1], Shohei Mori[2*], Mototaka Arakawa[1,2], and Hiroshi Kanai[1,2]

[1]*Graduate School of Biomedical Engineering, Tohoku University, Sendai, Miyagi 980-8579, Japan*
[2]*Graduate School of Engineering, Tohoku University, Sendai, Miyagi 980-8579, Japan*

[*]E-mail: mori@ecei.tohoku.ac.jp

Received December 2, 2020; revised February 10, 2021; accepted March 16, 2021; published online April 1, 2021

A measurement by transmitting ultrasonic non-focusing beams increases the temporal resolution but causes an error in the velocity measurements because of the lower signal-to-noise ratio (SNR) caused by the lower transmitted power and the lower spatial resolution. In the present study, we evaluated the relationship between the SNR and the transmitted beamwidth by the phantom experiment. The SNR decreased as the beamwidth became wider, and the measurement error increased when SNR was lower than 10 dB. Furthermore, the error factor due to the low spatial resolution more affected the measurement error than that due to the low transmitted power. © 2021 The Japan Society of Applied Physics

A diagnosis using echocardiography has the advantage of noninvasive and repetitive application compared with other diagnostic imaging methods. Ultrasonic measurement methods for the evaluation of cardiac function such as the characterization of the heart,[1)] the visualizations of the blood flow in the heart lumen,[2–4)] and the measurements of the propagation of the contraction on the myocardium,[5–9)] have been studied.

As myocardium dynamics are fast and complicated, high-resolution measurements are needed in both space and time domains. One of the techniques for obtaining the high temporal resolution in ultrasonic measurements is the method that an unfocused beam is sparsely transmitted and multiple focused receiving beams are formed from the received signals by the digital signal processing.[7)] However, in general, broadening the beamwidth of the transmitted wave causes the deterioration in the power of the transmitted wave at the local region and the spatial resolution, and the velocity measurement of the target medium is affected by the movements of neighboring tissues. Several methods have been proposed to improve the signal-to-noise ratio (SNR) and the spatial resolution in the measurement using the unfocused waves,[10–16)] and the beamforming performance has been quantitatively evaluated for a static object to confirm the usefulness of each method. Papadacci et al. quantitatively evaluated the relationship between the beamwidth of the diverging wave and the spatially averaged SNR of the shear wave velocity measurement.[11)] However, the relationship between the transmitted beamwidth and the error of the dynamic measurement has not been evaluated. The quantitative evaluation of the measurement accuracy in the dynamic motion of the target object remains an issue.

Furusawa et al. proposed a method[17)] to determine the optimal ultrasonic condition of transmitted beams for the measurement of the cardiac dynamic motion.[18)] The experimental system was constructed simulating the measurements of myocardial minute velocity, and the velocity estimation accuracies with several conditions of the transmitted beam were evaluated. However, the results were different as expected because the measurement error by the focused wave was larger than those by the plane and the diverging waves in the same frame rate condition. It is difficult to confirm the causes because the various error factors affected the evaluation.

Thus, it is necessary to evaluate the effect of each error factor independently. In our previous study, the effect of vibration frequency was examined. It was confirmed that the constructed experimental system can evaluate the measurement error of the target velocity moved by the sine wave of 50 Hz with an accuracy of approximately 2%.[19)]

The measurement error of the myocardial velocity is increased by the lower SNR, which is caused by the decrease of the power of the transmitted wave arrived at a region of interest and the deterioration of the spatial resolution. In the present study, we quantitatively evaluated the relationship among the transmitted beamwidth, the lower SNR caused by broadening the beamwidth, and the measurement error of the minute velocity. To evaluate each error factor, four types of experiments were conducted, (I) an experiment with no phantoms in a water tank, (II) an experiment with a target phantom A, (III) an experiment with a noise source phantom B, and (IV) an experiment with both of phantoms A and B. The phantoms A and B were placed at the positions shown in Fig. 1.

The measurement error was evaluated by comparing the velocity waveforms measured by ultrasound with the reference velocity waveforms measured by the laser Doppler velocimetry using the experimental system shown in Fig. 1. The vibration of the urethane phantom A was measured by ultrasound diagnosis equipment, and the velocity $\widehat{v_{\mathrm{U}}}(m)$ was obtained by applying the phased-tracking method[20)] to the central received beam. As the reference, the velocity $v_{\mathrm{L}}(m)$ was measured by a laser Doppler velocimetry. The measurement error $\sqrt{\overline{e^2}}$ by the ultrasound was calculated as

$$\sqrt{\overline{e^2}} = \frac{\sqrt{\sum_{m=0}^{M-1}\{\widehat{v_{\mathrm{U}}}(m) - v_{\mathrm{L}}(m)\}^2}}{\sqrt{\sum_{m=0}^{M-1}\{v_{\mathrm{L}}(m)\}^2}}, \tag{1}$$

where M is the number of samples in the velocity waveform.

We introduced the angular width θ_{w} to express the beamwidth,[17)] which was defined as

$$\theta_{\mathrm{w}} = 2\tan^{-1}\left(w\frac{r_{\mathrm{f}} - d_0}{2r_{\mathrm{f}}d_0}\right), \tag{2}$$

where r_{f} is the depth of focal point, w is the aperture width (19 mm), and d_0 is the target depth. The depth in Eq. (2) was fixed at 30 mm in the present study. The five different

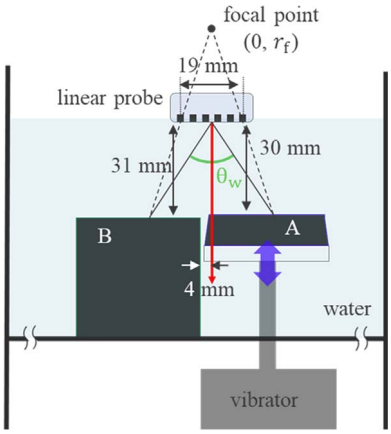

Fig. 1. (Color online) The schematic diagram of the experimental system and the definition of the transmitted beamwidth.

transmitted beamwidths were used: focused waves ($\theta_w = 5°, 21°$), a plane wave ($\theta_w = 35°$), and diverging waves ($\theta_w = 50°, 65°$). The objective of the present study was to evaluate the error factor caused by the lower power of the transmitted signal and/or the lower spatial resolution, the frame rate in each measurement was fixed at 3367 Hz which was sufficiently high to measure the target velocity with a vibration frequency of 50 Hz to avoid the error due to the temporal resolution.

First, the velocity of the target phantom A was measured in experiment (II) with only phantom A to evaluate only the error factor of the lower power of the transmitted wave as the wider beamwidth. Then, the error factor concerned with the lower spatial resolution in addition to that of the lower transmitted power was evaluated by measuring the velocity of the target phantom A in the experiment (IV) with phantoms A and B. The phantom B simulating a neighboring tissue has a different velocity component compared with the target phantom A.

The SNR and the error of the velocity measurement were calculated for 200 points in the range of depth d from 29.5 to 33.5 mm near the surface of phantom A at several beamwidths and with or without the phantom B. The SNR was calculated using Eq. (3) as $SNR_{\theta_w,d}$ by the ratio of the signal power from the measurement target A to the noise power from the other sources.

$$SNR_{\theta_w,d} = 10\log_{10}\left(\frac{1}{M}\sum_{m=0}^{M-1}\frac{\sum_{k=-K}^{K} w_k \cdot P_S(d+k)}{\sum_{k=-K}^{K} w_k \cdot P_N(d+k)}\right), \quad (3)$$

where M is the number of samples in the velocity waveform (673 points), K is the number of samples in the analysis window (32 points), w_k is the analysis window (Hanning window), and $P_S(d)$ (or $P_N(d)$) is the power of the received signal at the depth d from the measurement target A (or the other sources). $SNR_{\theta_w,d}$ related to the power of the transmitted wave was calculated by the power of the signal, $P_{S,A+water}$, measured in the experiment (II) with only phantom A and by the power of the noise, $P_{N,water}$, measured in the experiment (I) with no phantoms in the water tank. $SNR_{\theta_w,d}$ related to both the power of the transmitted wave and the spatial resolution was calculated by the power of the signal, $P_{S,A+water}$, measured in the experiment (II) with only phantom A and by the power of the noise, $P_{N,B+water}$, measured in the experiment (IV) with only the phantom B. In all conditions, the power was calculated from the signal obtained on the central received beam (red arrow in Fig. 1).

Radiofrequency data were acquired with a 7.5 MHz array probe (UST-5412, ALOKA, Japan) and the ultrasound diagnosis apparatus (Prosound α-10, ALOKA, Japan). The sampling frequency was 40 MHz. The laser Doppler velocimetry (LV-1300, Ono Sokki, Japan) and the oscilloscope (TBS2104, Tektronix, U.S.A.) were used for measuring the reference velocity of the surface of the target phantom A.

For simulating the in vivo measurement, a surface of the urethan phantom A was placed at depth of 30 mm from the probe surface and was vibrated up and down with a shaker (Type 4810, Brüel & Kjær, Denmark). The vibration frequency was set at 50 Hz. The urethane phantom B was set near the measured target phantom A as a neighboring tissue. The velocity of the phantom B was set as 0 mm s^{-1} (i.e. the phantom B was not moved) to set the different velocity compared with the measurement target phantom A.

The relationship among beamwidth, the measurement error, and the $SNR_{\theta_w,d}$ is shown in Fig. 2. In the experiment (II) using only the phantom A, there was a tendency that the $SNR_{\theta_w,d}$ decreased as the beamwidth broadened as shown in Fig. 2(a). The measurement error was small at the

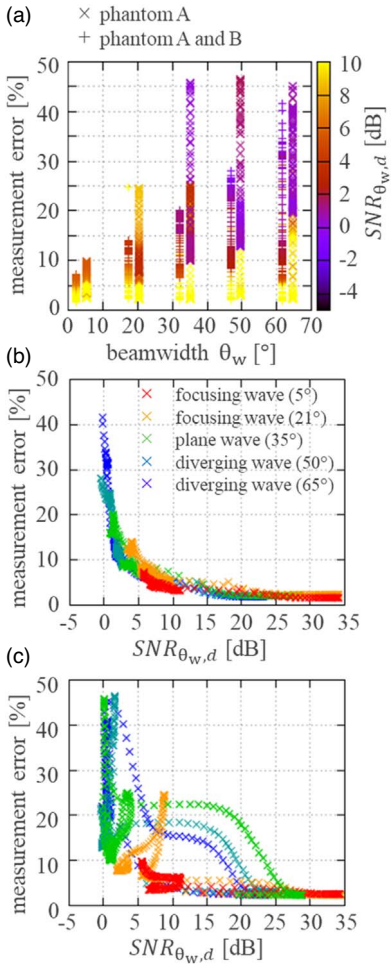

Fig. 2. (Color online) The relationship among the transmitted beamwidth, the measurement error of target velocity, and the $SNR_{\theta_w,d}$. (a) The comparison between the experiment with the target phantom A, and the experiment with the phantoms A and B, (b) the comparison among the five beamwidths in the experiment with the phantom A, (c) the comparison among the beamwidths in the experiment with the phantoms A and B.

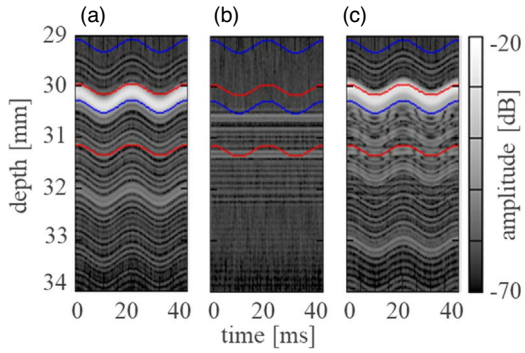

Fig. 3. (Color online) The M-mode images of the central received beam in the experiment with (a) the phantom A, (b) the phantom B, and (c) the phantoms A and B. The red and blue lines were analysis range when $SNR_{\theta_w,d}$ was 21.5 dB.

measurement depth where $SNR_{\theta_w,d}$ was higher than 10 dB and was large at the depth where $SNR_{\theta_w,d}$ was lower than 10 dB, regardless of the beamwidth θ_w as Fig. 2(b). In the case without phantom B, there were no other scatterer or reflector near the target phantom A and the frame rate was sufficiently high to measure the velocity with the vibration frequency of 50 Hz. These results suggest that the increase of the measurement error as the $SNR_{\theta_w,d}$ lower in the experiment (II) without the phantom B is due to the lower $P_{S,A+water}$, i.e. lower power of the transmitted wave arrived at a local region by broadening the ultrasound beamwidth.

In the experiment (IV) with both the target phantom A and the neighboring phantom B, $SNR_{\theta_w,d}$ was more decreased compared with that without phantom B. On some measurement depths, the results showed the same relationship between $SNR_{\theta_w,d}$ and the measurement error, however, the measurement errors exceeded 10% were obtained at the measurement depths with higher $SNR_{\theta_w,d}$ than 10 dB for beamwidths more than 5°, which was not observed in the experiment (II) without phantom B. In this case, the increase of the measurement error was caused by both the lower $P_{S,A+water}$ and the higher $P_{N,B+water}$.

To discuss the difference of the relationship of $SNR_{\theta_w,d}$ and the measurement error between Figs. 2(b) and 2(c), the M-mode images were compared. Figure 3 shows the M-mode images measured using the plane wave ($\theta_W = 35°$) for (a) only the phantom A [compatible with (II)], (b) only the phantom B [compatible with (III)], and (c) the phantoms A and B [compatible with (IV)], respectively. In Fig. 3(c), the interference pattern was observed at a depth deeper than 30.5 mm where the signal from phantom A in Fig. 3(a) and the signal from phantom B in Fig. 3(b) overlapped. In the region surrounded by red lines which includes interference pattern, $SNR_{\theta_w,d}$ was the same (21.5 dB) but the velocity measurement error was 11.0% larger compared with that surrounded by the blue lines (measurement error: 2.3%) which does not include the interference pattern. Thus, the velocity measurement error increased by the interference of scattered and/or reflected waves from the neighboring tissue with different velocity even in the condition that the measurement was less affected by the power of transmitted signals. These results suggest that the error factor due to the lower spatial resolution more affected the measurement error than that due to the lower power of the transmitted amplitude.

As the fundamental study, we quantitatively evaluated each error factor of the low transmitted power and the low spatial resolution, using the parameter $SNR_{\theta_w,d}$, depending on the transmitted beamwidth in the measurement of dynamic motion. The measurement error increased as the transmitted beamwidth broadening. The error factor of the lower spatial resolution affected the increase of the measurement error than that of the lower transmitted power. The measurement error of the focused wave was very low since the same frame rate was used as the diverging waves in the present experiment. However, the measurement error caused by the lower temporal resolution will increase when using focused waves because the measurements using the focused beams become a lower frame rate than those using the diverging beams. In the future study, we will determine the optimal transmitted conditions for dynamic measurements by additionally examining the error factor of temporal resolution which was not considered in the present study. The acceptable range of the measurement error for the dynamic measurement, which may depend on the dynamic property of the target tissue, will be also examined in future work.

Acknowledgments This work was supported in part by JSPS KAKENHI 19K22943.

1) K. Takahashi, H. Taki, and H. Kanai, Jpn. J. Appl. Phys. **56**, 07JF09 (2017).
2) M. Tanaka, T. Sakamoto, Y. Saijo, Y. Katahira, S. Sugawara, H. Nakajima, T. Kurokawa, and H. Kanai, J. Med. Ultrason. **46**, 413 (2019).
3) M. Maeda, R. Nagaoka, H. Ikeda, S. Yaegashi, and Y. Saijo, Jpn. J. Appl. Phys. **57**, 07LF02 (2018).
4) M. Mozumi, R. Nagaoka, and H. Hasegawa, Jpn. J. Appl. Phys. **58**, SGGE02 (2019).
5) H. Kanai, IEEE Trans. Ultrason. Ferroelectr. Freq. Control **52**, 1931 (2005).
6) M. Dandel and R. Hetzer, Int. J. Cardiol. **132**, 11 (2009).
7) G. R. Sutherland, G. D. Salvo, P. Claus, J. D'hooge, and B. Bijnens, J. Am. Soc. Echocardiogr. **17**, 788 (2004).
8) Y. F. Cheung, Nat. Rev. Cardiol. **9**, 644 (2012).
9) A. Hayashi, S. Mori, M. Arakawa, and H. Kanai, Jpn. J. Appl. Phys. **58**, SGGE05 (2019).
10) H. Hasegawa and H. Kanai, IEEE Trans. Ultrason. Ferroelectr. Freq. Control **55**, 2626 (2008).
11) C. Papadacci, M. Pernot, M. Couade, M. Fink, and M. Tanter, IEEE Trans. Ultrason. Ferroelectr. Freq. Control **61**, 288 (2014).
12) M. Correia, J. Provost, S. Chatelin, O. Villemain, M. Tanter, and M. Pernot, IEEE Trans. Ultrason. Ferroelectr. Freq. Control **63**, 420 (2016).
13) J. Grondin, V. Sayseng, and E. E. Konofagou, IEEE Trans. Ultrason. Ferroelectr. Freq. Control **64**, 1212 (2017).
14) S. Wang, W. N. Lee, J. Provost, J. Luo, and E. E. Konofagou, IEEE Trans. Ultrason. Ferroelectr. Freq. Control **55**, 2221 (2008).
15) M. Mozumi, R. Nagaoka, and H. Hasegawa, Jpn. J. Appl. Phys. **57**, 07LF23 (2018).
16) R. Nagaoka, M. Mozumi, and H. Hasegawa, J. Appl. Phys. **58**, SGGE10 (2019).
17) N. Furusawa, S. Mori, M. Arakawa, and H. Kanai, Jpn. J. Appl. Phys. **58**, SGGA08 (2019).
18) Y. Matsuno, H. Taki, H. Yamamoto, M. Hirano, S. Morosawa, H. Shimokawa, and H. Kanai, Jpn. J. Appl. Phys. **56**, 07JF05 (2017).
19) K. Sugahara, S. Mori, M. Arakawa, and H. Kanai, Proc. 41st Symp. Ultrason. Electron., 2020, p. 2Pb5-7.
20) H. Kanai, M. Sato, Y. Koiwa, and N. Chubachi, IEEE Trans. Ultrason. Ferroelectr. Freq. Control **43**, 791 (1996).